ESTIMATION OF STATISTICAL GEOMETRICAL PROPERTIES OF THE SURFACE OF ASTEROIDS FROM SIMULATIONS

E. THOUVENOT

Centre National d'Etudes Spatiales, DRT/TIT/RL, Toulouse Cédex, France

(Received 3 March; revised 10 October 1989)

Abstract. In order to evaluate the scientific feedback of a spaceborne radar in the frame of future space missions towards the asteroids, we present a method able to calculate mono-dimensional or two-dimensional simulations of the surface of any asteroid, or of the Moon.

A first set of results related to statistical geometrical properties of the surface, i.e. height and slope distributions, etc..., is given. Discussion shows that these results are in good agreement with observational data obtained from Earth for the Moon and for a few asteroids. In particular, we find r.m.s. slopes much greater on big asteroids than on the Moon.

1. Introduction

More than 50 asteroids have been observed by Earth-based radars since the first radar detection of Icarus in 1968 (Goldstein, 1968, 1969; Pettengill *et al.*, 1969). Since the intensity of the radar signal is very distance dependent, only two kinds of objects could be observed:

- Earth-grazing, Aten-Apollo-Amor asteroids, very small objects but studied at their closest approach to Earth;
- Main Belt asteroids, generally the largest ones in the Inner Main Belt detected at their opposition time.

Nevertheless, important scientific data were obtained for almost all these observed asteroids, concerning their shape, rotation period and axis, and surface roughness. In several cases, the signal to noise ratio was good enough to allow the determination of an evolution model of the backscatter coefficient with the incidence angle.

In order to study the primitive objects of the Solar System, the French and Soviet national space agencies (CNES and INTERCOSMOS respectively), studied an international mission called Vesta (Perret *et al.*, 1988). The Vesta mission is composed of two spacecraft which would fly-by about six to eight asteroids (from less than ten to several hundred kilometers in diameter) and two or three comets, at flyby velocities of several kilometers per second, and at distances at closest approach of about one to two thousand kilometers. A radar-altimeter-radiometer was planned for this mission, with a one-meter antenna working at 35 GHz (Raizonville *et al.*, 1988).

Scientific capabilities of such a radar are quite obvious, but have nevertheless

Earth, Moon, and Planets **48**: 1–34, 1990.

to be certified by very deep and precise analyses. Use of Earth-based observational data is of course possible for this, but two problems remain:

- these observations do not represent a significant sample of what the Vesta spacecraft could observe in the Main Asteroid Belt, especially for the small and medium-sized asteroids;
- the spatial and height resolutions of the radar will be much better than for Earth-based observations.

Since the scientific data obtained with the radar-altimeter aboard the Vesta spacecraft would be wholly derived from the received echoes, it seemed necessary to simulate asteroids of all diameters and types in order to compute the radar echoes that would be obtained; the processing of these echoes will then be determined and validated from this simulated data set.

One important point is to verify that simulated asteroids give the same global results as the real ones. So, comparisons with real data will be performed as often as possible to validate the models.

The way of obtaining radar echoes from simulated asteroidal surfaces, and discussion about computed echoes will be the subject of a forthcoming article. This paper presents the surface simulation method and gives the major geometrical results about simulated asteroids. The principle of the simulations will be discussed in Section 2. Section 3 will develop theoretical aspects of description of asteroidal surfaces. Results of one-dimensional simulations will appear in Section 4 and will be compared to observational data in Section 5. A small series of conclusions in Section 6 will complete this paper.

2. Principle of the Simulations

2.1. Background and hypotheses

Asteroids represent a very diversified population because of their different types and diameters. But their collisional history represents a major common point in their evolution. In fact, the absence of any geological evolution has not yet been proved. It is generally believed that asteroids several hundred kilometers in diameter may have been differentiated. Collisional fragmentation of such differentiated bodies could explain for example the existence of nearly entirely metallic asteroids. Debris caused by a very large number of impacts on asteroids may have formed a layer of material called regolith. We will see that regolith can't grow on asteroids where gravity is too small to retain any ejecta.

2.2. Proposed method

In our simulations, we will only consider the collisional evolution of asteroids. For the biggest ones, differentiation of the body may have partly melted the surface and obliterated existing craters, as on lunar maria. In this case, the simulations will refer to the non-melted part of the surface.

Of course, different types of asteroids will produce different kinds of cratering process and regolith evolution. We have chosen to describe three kinds of asteroids:

- weak bodies, that can represent carboneous asteroids;
- strong asteroids, corresponding to stony materials;
- very strong asteroids, with density and strength of metallic materials.

Even if the correspondence between these classes of asteroids and observational classes is not perfect, they will be called respectively C, S and M classes. Physical characteristics of these different types will be given thereafter.

To simulate the surface, we use a Monte-Carlo process; the surface is built step by step with craters chosen randomly in location and size, their shape depending on their size and on the type of the simulated asteroid. So. for a given asteroid, we propose the following scheme:

- to calculate the position of craters of any given diameter on its surface;
- to calculate the 'maximal crater', i.e. the largest crater caused by an impact that could almost destroy the asteroid;
- to calculate the mean depth of the regolith;
- to estimate the morphology of all craters, considered as fresh impacts;
- to take into account the difference between a 'fresh' and an 'old' surface, i.e. to include (i) obliteration of old craters by young ones, and (ii) erosion of each crater;
- to model the asteroid by including the regolith and all the simulated craters.

Prior to develop each of these points, it is important to define the spatial sampling of the simulations. In order to estimate the geometrical parameters of the surface for radar applications, it is theoretically necessary to know the surface to a $\lambda/10$ precision, where λ is the radar wavelength (e.g., Ulaby *et al.*, 1986). So, at 35 GHz, we would need a millimetric precision! Considering that it is nearly impossible to simulate any individual small pebble or boulder, a two-scale model will be used:

- the surface of the asteroid will be modelled with craters down to ten centimeters in diameter. At this scale, regolith will be considered as perfectly smooth;
- then the influence of the grain size distribution of the regolith, and of small pits will be estimated. For statistical reasons, boulders up to ten centimeters in diameter will be taken into account. In practice, as far as height and slope distributions are concerned, we will neglect larger boulders, because they are statistically rare at the surface of any asteroid. Data about a 'typical square meter' of any asteroid can be estimated from measures on terrestrial samples with appropriate materials and grain size distributions. This point will be discussed later.

We will see how to avoid prohibitive calculation times in simulating an asteroid

with a centimetric precision. The first step will be to do only mono-dimensional simulations, and to deduce two-dimensional properties of the surface from the mono-dimensional results.

3. Theoretical Aspects of Description of Asteroidal Surfaces

3.1. Crater densities on asteroids

If we neglect the particular localization of secondary craters, craters of all diameters will be randomly distributed on the surface of any asteroid. The number of craters between a given diameter D and $D + \mathrm{d}D$ per square kilometer is generally given by

$$\mathrm{d}N(D) = \alpha D^{\beta}\,\mathrm{d}D, \tag{1}$$

where α and β are constants.

Some authors prefer to speak in terms of cumulative densities, which represent the number of craters greater than D. After simplification, relation (1) yields

$$N_c(D) = \alpha_c D^{\beta_c}, \tag{2}$$

where

$$\alpha_c = -\alpha/(\beta + 1)$$

and

$$\beta_c = \beta + 1 .$$

Another notation is to give the number of craters in the interval $[D;\ 2^{1/2}D]$ (or sometimes $[2^{-1/4}D; 2^{1/4}D]$, that we will not use). In this case, we shall adopt an expression of the form

$$N_i(D) = \alpha_i D^{\beta_i}, \tag{3}$$

where

$$\alpha_i = -\alpha_c(1 - 2^{(\beta+1)/2})$$

and

$$\beta_i = \beta_c .$$

A straight line is then obtained when we plot these laws in log–log coordinates. Experimental results for different objects in the Solar System show that there is sometimes a break in the slope of this curve, which corresponds to the transition between the production density and the saturation density: for a given diameter of crater, so many impacts may have occurred that recent impacts have only obliterated older ones, leading to a limiting 'saturation' value for the density. The problem of saturation density has been discussed elsewhere (e.g., Hartmann,

1984). For asteroids in the Main Belt, we can assume that their highly collisional environment has created a 'near saturation' state for all diameters considered here. From values given for Phobos and Deimos (Thomas and Veverka, 1980), and for heavily-cratered surfaces in the Solar System (Hartmann, 1984), we will accept

$$\alpha = 0.177 (\log \alpha = -0.75) \quad \text{and} \quad \beta = -2.90 ,$$

which gives

$$\alpha_c = 0.093 (\log \alpha_c = -1.03) \quad \text{and} \quad \beta_c = -1.90$$

and

$$\alpha_i = 0.045 (\log \alpha_i = -1.35) .$$

An important remark is that this distribution seems unlikely to depend on the diameter and the type of the asteroid. In fact, the distribution of impacting bodies is constant in the Asteroid Belt. We can assume that the mean relative impact velocity is a constant too. But, for a given impacting body, the diameter of the resulting crater would depend on the strength and sometimes on the gravity field of the target asteroid, too (cf. Equation (4)). However, the concept of saturation density leads us to assume that this distribution is the 'maximal' one, and that it is the same for all types of asteroids. Of course, there will be a limitating value for each asteroid corresponding to the disruption of the body. That is the subject of the following section.

3.2. The maximum diameter

We can write an expression which relates the crater diameter to the energy of the impact (e.g., Housen, 1981; Housen and Wilkening, 1982)

$$D = K_D E^{\delta} h(g) , \tag{4}$$

where K_D depends only on the strength S_0 of the material of the asteroid, δ is a parameter which depends on the cratering regime, and $h(g)$ is function of the gravity g of the asteroid

$$g = \gamma \rho \phi , \tag{5}$$

where ϕ is the diameter of the asteroid, ρ is its density (we consider homogeneous, non-differentiated asteroids), and γ is a constant that can be easily calculated by using relation (5) with Earth values. In order to be consistent with the literature, we will use the c.g.s. system to formulate the following equations, but constants and results will be given in the metric system as often as possible.

The cratering regime is characterized by the f number which is defined (cf. Gault and Wedekind, 1977) as

$$f = S_0 / \rho g D . \tag{6}$$

When $f \gg 1$, material strength dominates gravitational forces, and such a regime is called 'strength-scaling' regime;
When $f \ll 1$, gravitational forces predominate and we have a 'gravity-scaling' regime;
When $f \approx 1$, we are in a transitional regime. We will note D_f the crater diameter for which $f = 1$.

The expression of $h(g)$ is then:

$$\text{in strength-scaling} \quad h(g) = 1 \tag{7a}$$

$$\text{in gravity-scaling} \quad h(g) = g^{-1/6} . \tag{7b}$$

Let E_d be the minimum energy required to disrupt the asteroid (it is smaller than the minimum energy required to disperse the fragments, but we will not take re-accretion process into account). We can write

$$E_d = S_1 V_\phi = \pi S_1 \phi^3/6 , \tag{8}$$

where V_ϕ is the volume of the asteroid and S_1 is its 'average ultimate strength': strength of materials increases with the pressure related to an impact. This factor of increase may reach 10^4 to 10^5 in certain cases of asteroidal impacts. So, S_1 may be defined as the average strength of the asteroid due to destructive impact. It can be shown (Davis *et al.*, 1985) that

$$S_1 = S_0 + \pi G k \rho^2 \phi^2/15 , \tag{9}$$

where G is the gravitational constant, and k is a constant that will be taken equal to 1.

Combination of Equations (4) to (9) leads to calculate the maximal diameter D_M for a given asteroid. The constants that we will use for the different types of asteroids will be:

for C-type asteroids: $\rho = 2.0 \text{ g cm}^{-3}$ and $S_0 = 10^4 \text{ N m}^{-2}$,
for S-type asteroids: $\rho = 3.5 \text{ g cm}^{-3}$ and $S_0 = 3 \times 10^6 \text{ N m}^{-2}$,
for M-type asteroids: $\rho = 6.0 \text{ g cm}^{-3}$ and $S_0 = 10^8 \text{ N m}^{-2}$.

The constants K_D and δ have been estimated for weak and strong materials (e.g., Housen, 1981). We have tentatively extrapolated these values for very strong materials. So, for:

C-type asteroids: for gravity-scaling: $K_D = 8.00 \times 10^{-3}$ and $\delta = 0.333$
for strength-scaling: $K_D = 6.36 \times 10^{-2}$ and $\delta = 0.290$
S-type asteroids: for gravity-scaling: $K_D = 2.75 \times 10^{-3}$ and $\delta = 0.333$
for strength-scaling: $K_D = 4.20 \times 10^{-2}$ and $\delta = 0.290$

M-type asteroids: for gravity-scaling: $K_D = 1.0 \times 10^{-3}$ and $\delta = 0.333$
for strength-scaling: $K_D = 2.0 \times 10^{-2}$ and $\delta = 0.290$.

Equations have to be solved by assuming that the maximal diameter will correspond to a given regime. If this is not verified, the regime is changed, and if no regime is applicable, we average the two values. It is interesting to note that, as a consequence of the two cratering regimes, the maximal diameter of weak bodies is smaller for small asteroids, and greater for large asteroids, than the maximal diameter of strong bodies. The regime changes when ϕ is, respectively, about equal to 5, 50, and 200 km for weak, strong and very strong asteroids. The results will be shown on Figure 3.

3.3. Mean depth of the regolith

The problem of the evolution of asteroidal regolith has been dicussed elsewhere. Main models in the literature are the Housen *et al.*, model (Housen *et al.*, 1979a,b; Housen, 1981; Housen and Wilkening, 1982), and the Langevin and Maurette model (Langevin and Maurette, 1980, 1981, Langevin, 1982, 1986). In this section, we will attempt to determine the mean depth of the regolith with a simple analytical model. We will not calculate local variation of the regolith thickness. Of course, we will consider that the thickness to asteroid diameter ratio is very small.

The regolith growth is due to the formation of ejecta from impact cratering. So, it is important to know what is the fraction of ejecta that falls back on the asteroid surface. In fact, ejecta with initial launch speed greater than the escape velocity of the asteroid will never participate to the growth of the regolith (except if a third body creates gravitational perturbations of the trajectory of the escaped ejecta, as it could have been the case for the Martian satellites (Soter, 1971). We suppose that it is not the case here).

For a given crater, the fraction of ejecta with launch speed greater than v has been given by Langevin et Maurette (1980)

$$\chi(v) = (v_r/v)^2 , \tag{10a}$$

where v_r is the ejecta velocity at the crater rim.

The exponent of this law has been discussed by Housen (1981), but the nominal value is generally believed to be very close to 2. Uncertainties mainly come from the asymptotic variations of χ (in a log–log plot) when v tends to very small values. So, a better model would be

$$\chi(v) = (1 + (v/v_r)^2)^{-1} , \tag{10b}$$

which is of the same form as the model proposed by Langevin (1982). Of course, expressions (10a) and (10b) differ only for small values of (v/v_r).

The assumed expressions for v_r are:

for strength-scaled craters,

$$v_r = 0.18 S_2^{0.55} ; \tag{11a}$$

for gravity-scaled craters,

$$v_r = (gR/6)^{1/2} ; \tag{11b}$$

where S_2 is the cohesive strength of the target material, and R is the crater radius. To be consistent with the literature, S_2 has to be taken between S_0 and S_1. We will choose $S_2 \approx 5S_0$ (Housen, 1981). This value would be much lower for impacts in the regolith itself. But, we will see that the most important craters are large enough to reach the bedrock under the regolith.

Experimental data have shown that expression (11a) describes also the gravity-scaled craters.

The expression of the escape velocity at the asteroid surface is

$$v_e = (g\phi)^{1/2} . \tag{12}$$

Thus the fraction of ejecta which escapes the asteroid is

$$F = (1 + g\phi/v_r^2)^{-1} . \tag{13}$$

Figure 1 shows the difference for the F factor when applying relation (11a) to (10b) or (10a).

The $(1 - F)$ fraction of ejecta falls on to the surface and participates to the growth of the regolith. The volume of ejecta produced by an impact crater may be approximated by the volume of a spherical cap. If the depth to diameter ratio is x, the corresponding volume is

$$V = \pi x(3 + 4x^2) D^3/24 . \tag{14a}$$

We will see in the following section that a good approximation can be made by choosing $x = 0.2$. Therefore,

$$V = \nu D^3 , \tag{14b}$$

where $\nu \approx 8.27 \times 10^{-2}$.

The total volume of ejecta produced by craters with diameters between D and $D + \mathrm{d}D$ is

$$\mathrm{d}^2 V_T = V \, \mathrm{d}N \, \mathrm{d}S = \nu\alpha D^{\beta+3} \, \mathrm{d}D \, \mathrm{d}S . \tag{15}$$

The total volume of ejecta created by all craters between D_0 and D_S (with $D_0 \ll D_S$) can be expressed by

$$\mathrm{d}V_T = \nu\alpha/(\beta + 4) D_S^{\beta+4} \, \mathrm{d}S . \tag{16}$$

The problem is to define the proper limit for this integration. The choice of D_S

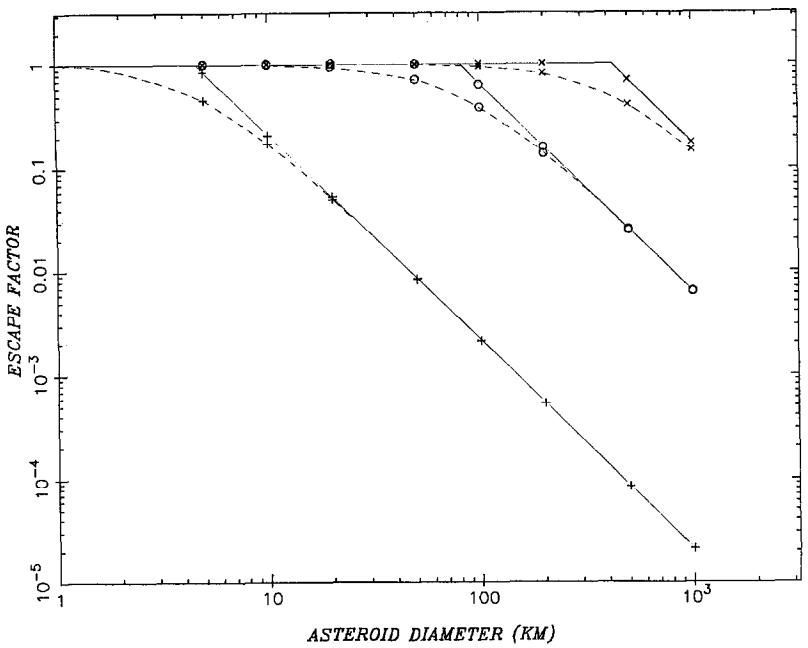

Fig. 1. Evolution of the escape factor F for strength-scaled craters with the asteroid diameter. For all figures, data concerning C-type, S-type, and M-type asteroids will be respectively represented with plus signs, open circles, and crosses. For each asteroid type, the top curve (solid line) corresponds to the Housen model, and the bottom curve (dashed line) is from the Langevin model.

is determined from geometrical considerations about ejecta distribution that we present thereafter.

By integrating Equation (16) among all the asteroid surface, and taking the $(1 - F)$ fraction of this volume, we find the total volume of produced ejecta for the asteroid to be given by

$$V_T = \pi(1 - F)\nu\alpha/(\beta + 4)D_S^{\beta+4}\phi^2 . \tag{17}$$

One important hypothesis is then to suppose that this volume of ejecta is uniformly distributed among the asteroid surface. In fact, this supposes that, for any given diameter between D and $D + \mathrm{d}D$ (and not for any individual crater), the corresponding ejecta is uniformly distributed. D_S will be defined as the crater diameter for which a non-negligible part of its total ejecta does not recover uniformly all the asteroid.

If δ_r is the mean depth of the regolith, we can calculate the total volume of regolith on the given asteroid: i.e.,

$$V_R = \pi\phi^2\delta_r . \tag{18}$$

The definition of D_S allows us to write that $V_T = V_R$, and the final expression of

the depth of the regolith becomes

$$\delta_r = (1 - F)\nu\alpha/(\beta + 4)D_S^{\beta+4} . \tag{19}$$

The last unknown parameter in this equation is D_S.

For a given impact, the fraction of volume of non-escaped ejecta which falls on to the surface at distances from the center of the crater from r_m (minimal range of the ejecta) to r is:

$$y = 1 - r_m/r . \tag{20}$$

So the fraction of 'forgotten' volume when we proceed to integration until r instead of the infinite is

$$\tau = r_m/r . \tag{21}$$

Let D_{ES} be the saturation diameter of ejecta related to the saturation diameter D_S. We have

$$D_{ES} = 2r_{ms}/\tau_s . \tag{22}$$

The definition of D_S implies that the total elementary surface, covered by the ejecta of craters of diameters between D_S and $D_S + dD$, reaches the surface of the asteroid. So the conditions can be written as

$$\alpha D_S^{\beta}\pi\phi^2(\pi D_{ES}^2/4 - \pi r_{ms}^2) = \pi\phi^2 ;$$

so that

$$\pi\alpha D_S^{\beta} r_{ms}^2(\tau_s^{-2} - 1) = 1 . \tag{23}$$

In gravity-scaling, $r_m = D/2$, so that

$$D_S = [\pi\alpha(\tau_s^{-2} - 1)/4]^{-1/(\beta+2)} . \tag{24}$$

In this case, the saturation diameter does not depend on the asteroid. In practice, this value will be used to calculate the asymptotical depth of the regolith (when $F \to 0$).

In strength-scaling, $r_m = D/2 + v_r^2/g$ so that

$$\pi\alpha D_S^{\beta}(D_S/2 + v_r^2/g)^2(\tau_s^{-2} - 1) = 1. \tag{25}$$

This relation can be easily solved by using a dichotomy method.

The estimate of τ_s is a critical point. An empirical choice would lead to a value between 10% and (say) 30%. A physical choice should be preferable, and this is why we will suppose that the calibration of the method will be determined by a case where the depth of the regolith is relatively known: i.e., the Moon.

The Moon has approximatively the same physical characteristics as a S-type asteroid. The mean depth of the regolith is about 5 m. The crater density is certainly not the same as for the asteroids: for considered impacts, the heliocentric

velocities are about three times greater for the Moon ($\approx 15\,\mathrm{km\,s^{-1}}$) than in the Asteroid Belt ($\approx 5\,\mathrm{km\,s^{-1}}$) (e.g., Hartmann, 1977).

So this different speed will give different energies of impact ($E \alpha v^2$), and then different crater diameters ($D \alpha E^{\delta}$). Moreover, the number of impacting bodies is believed to be 30 to 50 times lower for the Moon than for the Asteroid Belt, with about the same shape in the mass distribution (Langevin and Maurette, 1980; Housen, 1981).

We assume (our assumptions will be verified effectively) that:

- firstly that the saturation diameter does not correspond to the production zone, so we can keep $\beta \approx -2.9$.
- secondly that this saturation diameter corresponds to strength scaling, so $\delta = 0.333$.

In this case, we can estimate the α parameter for the Moon, which is between 4 and 6 times lower than for the asteroids. This correponds to values generally found in the published data for the Moon (e.g., Hartmann, 1984). Then, assuming that $F = 0$, which is obvious for the Moon, we can calculate the saturation diameter (several hundred meters), which yields:

$$\tau_s \approx 0.25 .$$

This value is in the supposed interval, and we will use it for all the other cases.

Results about δ_r are shown in Figure 2. Obtained values are smaller than in the

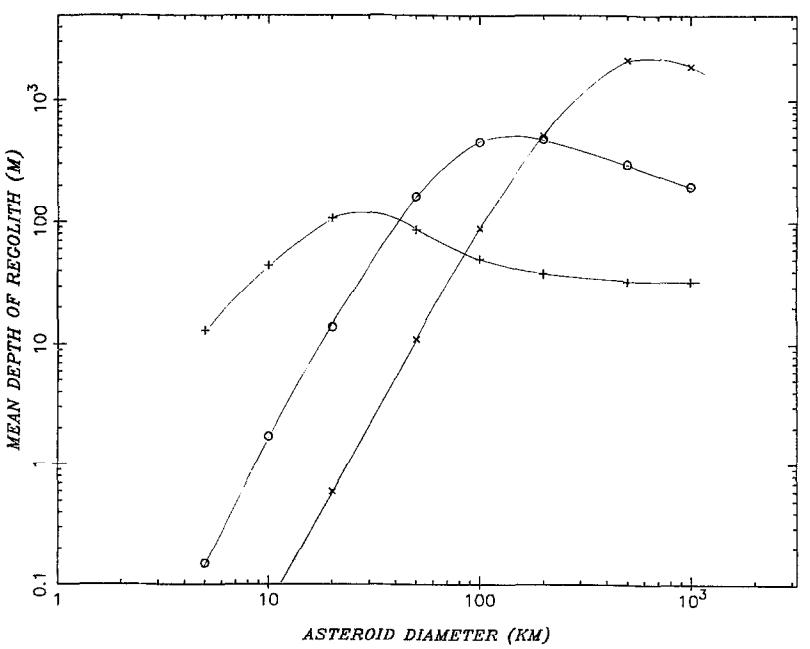

Fig. 2. Mean depth of regolith for asteroids between 5 and 1000 km in diameter. Note the maximum value for each asteroid type, and the asymptotical tendency for C-type asteroids.

Housen model, and are much closer to the Langevin and Maurette values. It is interesting to notice that, for a given type of body, there is a diameter of asteroid for which the depth of the regolith is maximum: for smaller asteroids, there is more escaping ejecta, and for larger asteroids, gravity concentrates ejecta in the proximity of most craters.

Craters morphologies

Craters morphologies have been widely studied on the Moon (e.g., Pike, 1977; Wood and Andersson, 1978; Croft, 1985; Ravine and Grieve, 1986). Some analyses on Martian satellites exist too (cf., Turner, 1978; Veverka, 1978). We will not use results about Mars or icy satellites because of their particular cratering process.

Based on these studies, it seems possible to determine what will be the approximative morphology of any considered crater for any type of asteroid. We will consider in this section that all these craters are fresh. We will simulate neither terraces the existence of which is not certain on large craters on large asteroids, nor centrals peaks which are negligible here for slope and height distributions. The general shape of a crater is represented in Figure 4. We will note that

- D_c its internal diameter (rim to rim) (and R_c its radius);
- d its total depth: $d = p + h$, where p is the depth below the zero-level and h is the rim height;
- F the diameter of its (eventual) flat floor (and f its radius);
- R_F its rimwall width;
- D_t its total diameter ($D_t = 2R_t$; $R_t = R_c + R_F$).

We will distinguish three main types of craters, on the assumption that the body is non-differentiated:

(a) $D < 5\delta_r$.

Small craters are entirely in the regolith. They are characterized by a paraboloid shape (bowl-shaped craters), and are entirely below the surface level. The depth to diameter ratio is near 0.2 for the Moon as well as for Martian satellites. This class will concern all craters with diameter smaller than about $5\delta_r$. As the minimum crater diameter in our simulations is 10 cm, this class will only exist if δ_r is superior to 2 cm in depth.

The two other types will depend on the cratering regime. In practice, the transition diameter D_T between strength-scaled crater and gravity-scaled craters will not exactly be equal to D_f. It would be more appropriate to say that between D_f and D_T, the morphology of craters is closer to the second type than to the third one. The analysis of data suggests that $D_T \approx 2D_f$ for C-type asteroids and $D_T \approx 3D_f$ for S-type asteroids. So we will take $D_T \approx 5D_f$ for M-type asteroids. This gives a transition diameter for the Moon at about 16 km, which corresponds to the observed value between 15 and 20 km. The shape of D_T evolution for all

C-TYPE ASTEROIDS

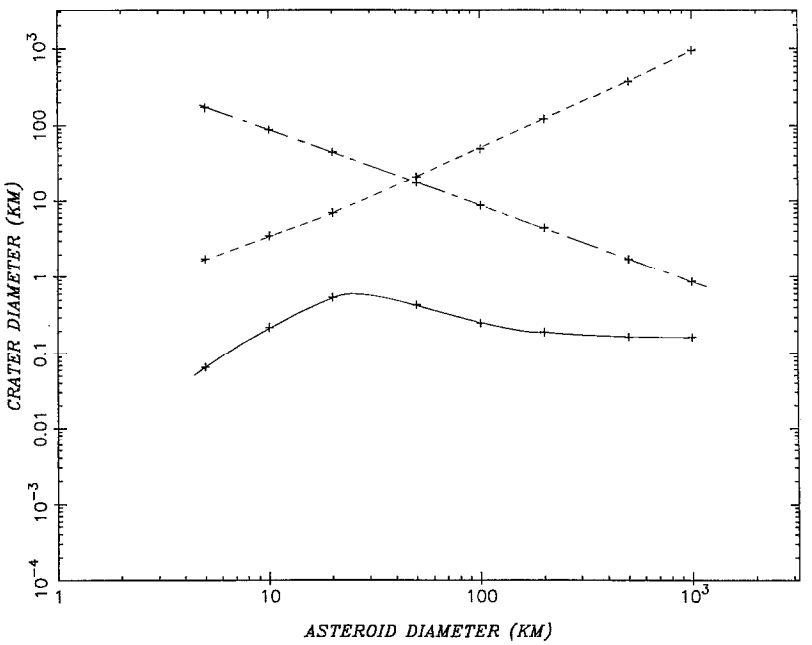

Fig. 3a.

S-TYPE ASTEROIDS

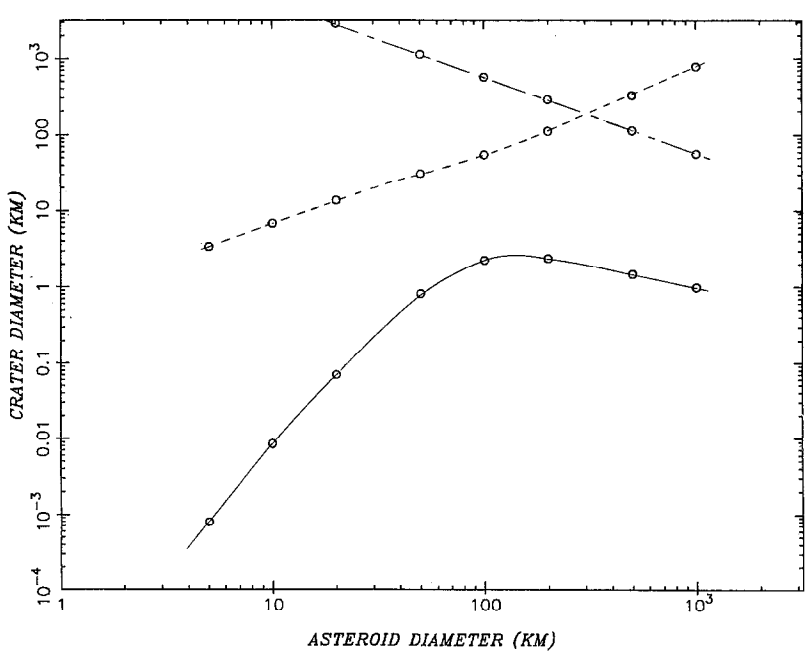

Fig. 3b.

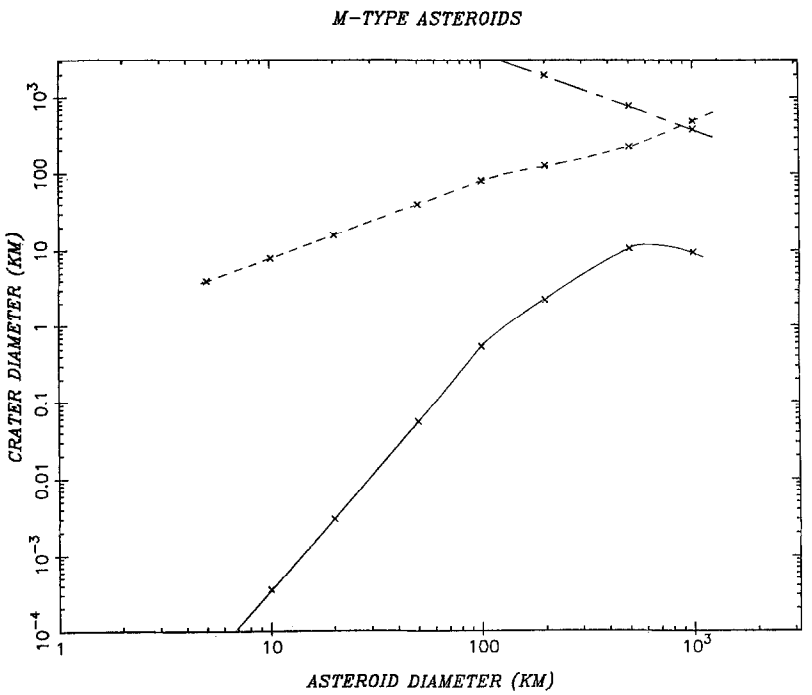

Fig. 3. Limiting values of craters for C-type (3a), S-type (3b), and M-type (3c) asteroids. The minimum considered crater diameter is 10 cm. Solid lines, dashed lines and chain-dotted lines correspond repectively to $5\delta_r$, D_M and D_T.

types of asteroids is represented in Figure 3. We can now describe the two last types:

(b) $\quad 5\delta_r < D < D_T$.

Craters are nearly bowl-shaped, but with a small flat floor. Their rim-wall goes just a little above the surface, and still has a paraboloid shape. Experimental data show that the height of rim-flank decreases with the third power of the distance to the center.

(c) $\quad D_T < D < D_M$ (if $D_T < D_M$).

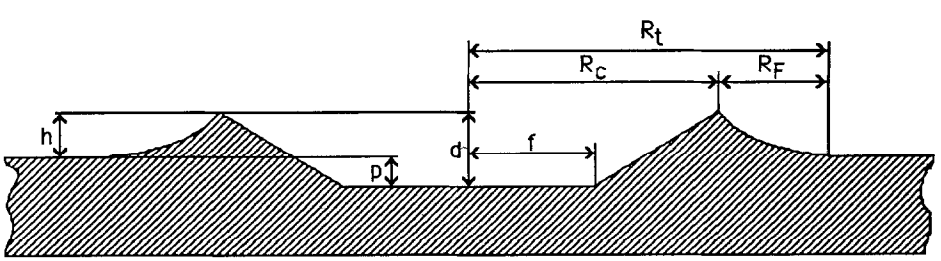

Fig. 4. General cross-section of a crater (see the text for notations).

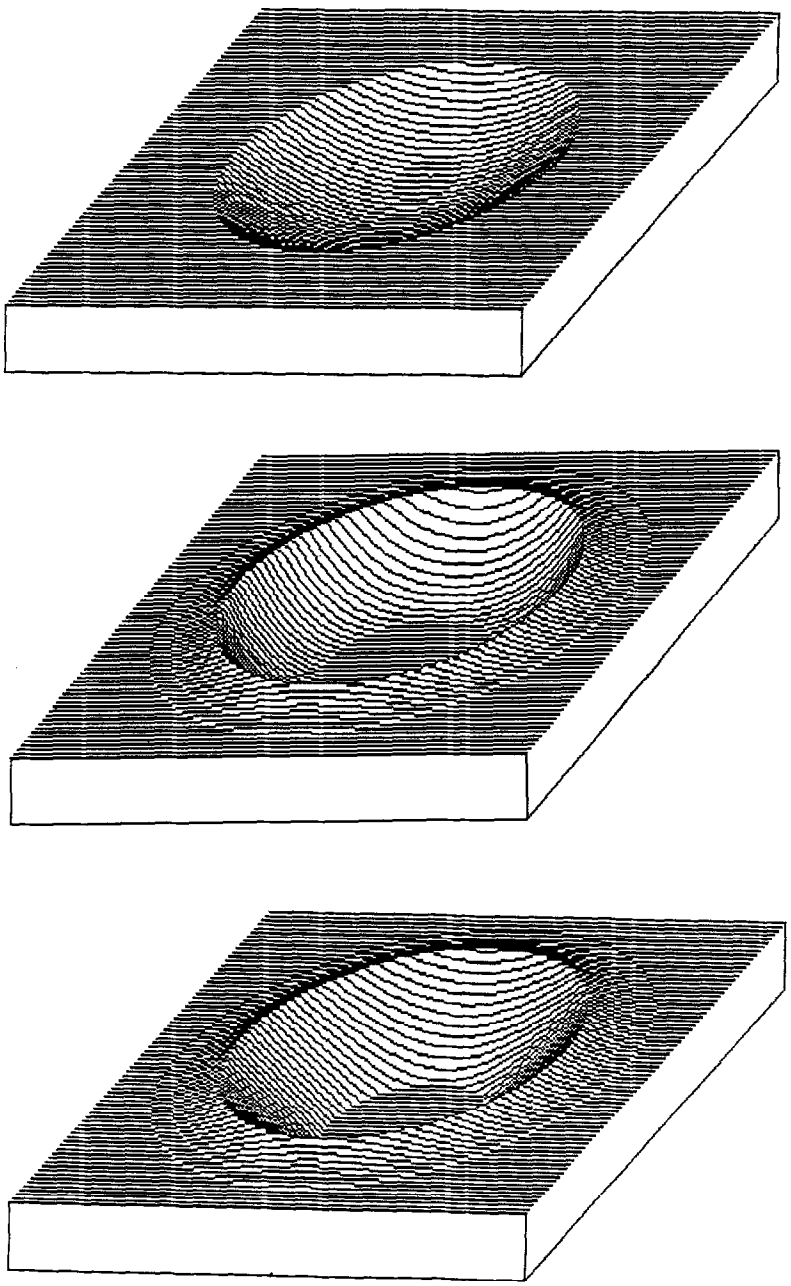

Fig. 5. Three-dimensional aspect of the three types of craters. Vertical reliefs are exaggerated. The crater diameter is normalized to D_T. (i) above: small, bowl-shaped craters. (ii) middle: intermediate, bowled-shaped craters with small flat floors and rims. (iii) bottom: great craters with important flat floors and flat rim-walls.

TABLE I

Geometrical properties of craters

Crater type	a	b	c
	(if $\delta_r > 2$ cm)		(if $D_T < D_M$)
Diameter	10 cm $< D_c <$ 5δ_r	5$\delta_r < D_c < D_T$	$D_T < D_c < D_M$
p/D_T	$0.196(D_c/D_T)$	$0.196(D_c/D_T)$	$0.196(D_c/D_T)^{0.301}$
h/D_T	0.	$0.08g_r^{0.208}(D_c/D_T)$	$0.08g_r^{0.208}(D_c/D_T)^{0.399}$
F/D_T	0.	$0.445(D_c/D_T)^{1.765}$	$0.445(D_c/D_T)^{1.249}$ ($F_M = 0.985D_T$)
R_F/D_T	0.	$0.267(D_c/D_T)^{1.011}$	$0.267(D_c/D_T)^{0.836}$

Craters greater than D_T in diameter correspond to usual big (but not complex) lunar craters: the flat-floor is more important than in the precedent type, the depth to diameter ratio decreases with increasing diameter, rim-walls are approximately flat, and rim-flanks have the same shape as for the previous case.

The three different types of craters are represented in Figure 5. For this Figure, vertical relief is exaggerated, and all diameters are normalized to D_T.

The geometrical parameters for each type of crater are given in Table I. In this Table, g_r corresponds to the gravity of the asteroid relative to Earth (the height above the zero-level depends on the gravity at the surface of the body). For the flat floor diameter of the last type of crater, we used a fixed limiting value relative to the diameter of the crater (which is related to the maximum slope of the rim-wall for lunar craters).

Equations of craters appear in Table II.

3.5. Crater erosion

In the preceding section, we studied the morphology of a fresh crater – i.e., whose impact has just occurred. We will now describe the direct effects of any impact crater (down to 10 cm in diameter) on the substratum, which causes progressive eradication of old craters by new ones. In this section, other factors will be taken into account: impacts due to very small bodies (giving craters smaller than 10 cm

TABLE II

Equations of craters

Type	Radius	Equation
a	$0 < r < R_c$	$z/d = -1 + (r/R_c)^2$
b	$0 < r < f$	$z = -p$
	$f < r < R_c$	$(z-h)/d = -1 + [(r-f)/(R_c-f)]^2$
	$R_c < r < R_c + R_F$	$z/h = (R_c + R_F - r)^3/R_F^3$
c	$0 < r < f$	$z = -p$
	$f < r < R_c$	$z = d(r - R_c)/(R_c - f) + h$
	$R_c < r < R_c + R_F$	$z/h = (R_c + R_F - r)^3/R_F^3$

in diameter), micro-impacts, and influence of the distribution of ejecta for all impacts.

In fact, the distribution of ejecta is influenced by the local slope. For example, ejecta will not be uniformly distributed for an impact which occurs on the rimwall of a bigger crater. In this particular case, a small part of ejecta could hardly reach the edge of the rimwall, while the greater part could go down the slope and reach the crater floor.

When we consider the global effect of all impacts on any given crater, it may be described by an erosion, which slowly smoothes slopes and reduces height extremas. It may be shown (Langevin, 1988, private communication), that the mathematical modelling of such an erosion yields a Laplacian form

$$\partial z/\partial t = \epsilon(\partial^2 z/\partial x^2 + \partial^2 z/\partial y^2) \tag{26}$$

where ϵ is a parameter (e.g., in square kilometer per gigayear) which will describe the importance of the erosion. The erosion will depend on time and on the area of the considered crater. Expression (26) may be easily written in a discrete and iterative form. To describe all stages of erosion with enough precision, and to obtain a compromise between the precision of the algorithm and the computer time, we have finally chosen to simulate very old craters with fifty iterations.

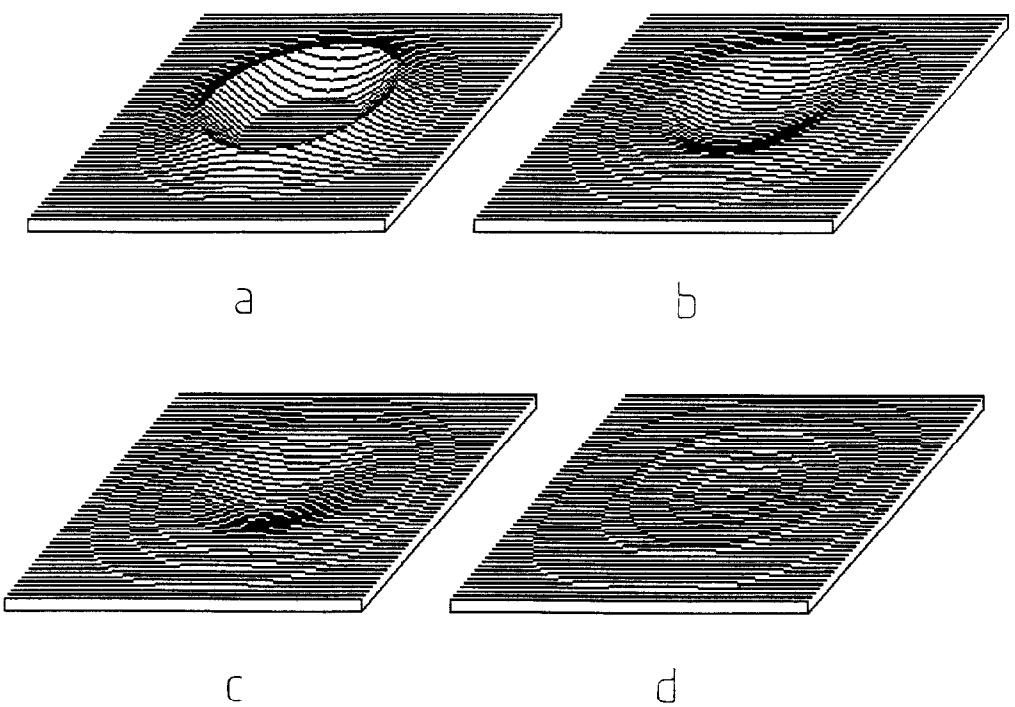

Fig. 6. Three-dimensional aspect of a fresh (a), young (b), mature (c) and old (d) crater. Vertical scale is nearly not exaggerated if we consider that $g_r \approx 0.1$.

Although a theoretical approach was possible, the adjustment of the ϵ parameter was done so that the most eroded craters have the same aspect as very old lunar craters. Figure 6 shows the three-dimensional aspect of fresh (a), young (b), mature (c), and old (d) craters. This corresponds, respectively to zero, ten, twenty and fifty iterations in the numerical algorithm. The nomenclature is from Moore *et al.* (1980), who defined the absolute and relative abundances of these classes for small lunar craters (with up to seven morphologic types). Information about degradation of bigger craters can be found elsewhere (e.g., Malin and Dzurisin, 1977). When the number of iterations (i.e., $\approx$ the age) of the algorithm is randomized, relative abundances of eroded crater types fit very well with Moore *et al.*'s data.

3.6. Craters obliteration

When we want to 'superimpose' a new crater to an old one, we must take into account the influence of preexisting morphology. This morphology will not be affected beyond the limit of rim flank (as defined in Section 3.4), while the effect will be maximum at the center of the crater (i.e., the location of the impact) (e.g., Helfenstein, 1988). Then we can intuitively define the final uplift as a linear combination of the preexisting and of the new crater heights of the form

$$z_f(r) = \phi(r) z_p(r) + (1 - \phi(r)) z_n(r) , \tag{27}$$

where $z_f(r)$, $z_p(r)$, and $z_n(r)$ are, respectively, the final height, the old one, and the elevation of the new crater, at a distance r from its center, and $\phi(r)$ is a parameter that has to be defined. In this simple model, we suppose that $\phi(r)$ does not depend on the cratering regime.

A general expression for $\phi(r)$ will be

$$\phi(r) = (r/R_T)^{\psi} . \tag{28}$$

A somewhat more complicated expression is proposed by Langevin (1988, private communication), with two horizontal tangents for $\phi(r)$ at $r = 0$ and $r = R_T$. A physical approach of the impact would perhaps provide the ψ parameter. between 0.5 and 3 seem reasonable, and changes in the final aspect are nearly indistinguishable. However, comparisons of two-dimensional simulations with lunar images made us choose $\psi = 2$.

4. Simulations

4.1. Mathematical approach

There are more than seven decades between the diameters of the smallest craters to simulate and the biggest ones, and about 15 decades between their respective abundances. So, it is not a priori possible to simulate all these craters.

The first idea is to make only mono-dimensional simulations – i.e., to simulate a 'line of an asteroid'. Of course, two-dimensional simulations were previously done to validate the model, but only with less resolution, or on a very small area.

The second idea is to 'fractalize' the profile: The smaller craters will be only simulated on a limited length, which will be repeated, here ten times, at a greater scale where will be included greater craters, etc... in practice, craters will be simulated in intervals of the form $[D_i; 2^{1/2}D_i[$, which will be called the i-th interval, where $D_1 = 10$ cm, and $D_i + 1 = 2^{1/2}D_i$. The number of craters in each interval will be determined, and it is possible to show that the diameter of each crater in a given interval can be determined by:

$$D = D_i[1 - w(1 - 2^{(b+1)/2})]^{1/(b+1)}, \tag{29}$$

where w is a random number with an uniform density in the interval [0; 1]

There will be a special processing for the last interval (i.e., the interval containing the largest crater for a given asteroid).

Figure 7 shows the basic concept of these simulations. The problem is to define the dimension of each Table so that computing time is not prohibitive. Statistical constraints may be:

- the smallest crater in a Table must be sampled with at least ten points;
- there must be a minimum number (say, ten) of simulated craters for the last interval of each table (except for the biggest craters on the asteroid).

Several attempts were done. The found optimization is to use 5 tables, with 100000 elements in each table. Thus, it represents:

- a 1 km line, with a 1 cm step, which contains the eight first intervals (from $D_i = 10$ cm to $D_i = 1.13$ m);
- a 10 km line, with a 10 cm step, which contains the following eight intervals (from $D_j = 1.6$ m to $D_i = 18.1$ m);
- a 100 km line, with a 1 m step, which contains the following eight intervals (from $D_i = 25.6$ m to $D_i = 290$ m);
- a 1000 km line, with a 10 m step, which contains the following seven intervals (from $D_i = 410$ m to $D_i = 3.28$ km);
- a 10000 km line, with a 100 m step, which contains the last fifteen intervals (from $D_i = 4.63$ km to $D_i = 593$ km).

The first statistical demand is thus respected. For a given diameter interval i the corresponding line I_j can be influenced by craters at distances up to $L_j = R_{i+1} + RF_{i+1}$ on each side of the line. The total number of craters to simulate for this interval will be (from (3))

$$n_i = 2L_iI_j\alpha_{inc}D_i^{\beta+1}. \tag{30}$$

Thus it is possible to verify that the number of craters in the last interval of a given line is more than 10, except for very large craters, – in the fifth line –, which can hardly exist on very big asteroids. The position of each crater along the line will be determined by a random number (with a uniform distribution). The total

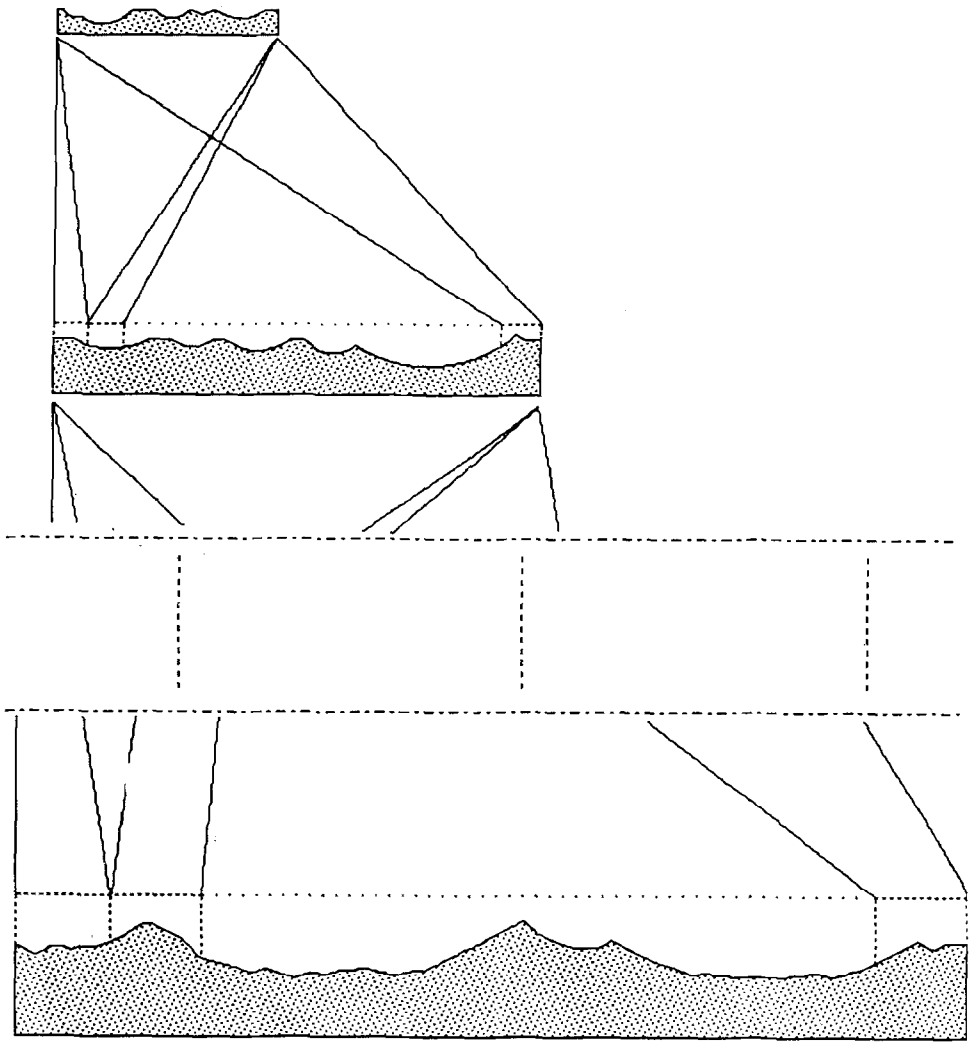

Fig. 7. Principle of the simulations: models for smaller scales are introduced and repeated in greater scales. Optimization (see the text) yields a factor 10 between each stage, and 5 successive stages.

number of craters for each line is about 1000, which is very small and possible to simulate.

Each line will be simulated using theories developed from Section 3.1 to Section 3.6. Parts of craters which are out of the limits of a simulated line at one end will not be eliminated but transferred at the other end, in order to avoid problems when connecting a line to itself. For all considered asteroids, the total simulated "pseudo-line" will be 10000 km long. That is of course much longer than the perimeter of the asteroid, but very useful to obtain good statistical results.

The 'pseudo-table' corresponding to the pseudo-line contains 10^9 elements

(10000 km with 1 cm step). The altitude of each element will be obtained by the combination of the altitudes of the 5 simulated lines at the correct places. Linear interpolations will be used to determine the altitude between two points when the step is greater than 1 cm, i.e., in the last 4 lines.

Simulations have been made on CDC 990/VE and 992/VE computers. Each line requires about 10 sec CPU, and obtaining statistical results for the pseudo-tables takes about 3000 sec CPU.

These results relate to:

(i) Heights

The program gives mean height $\bar{h}$ and r.m.s. height h_{rms}. Height distribution is also calculated;

(ii) Slopes

As mean slope is zero, the program gives $|\bar{\theta}|$, i.e., the mean of absolute values of slopes, and r.m.s. slope θ_{rms}. Slope distribution is given too. In fact, we give the distribution of the angles (in degrees), and the distribution of the slopes (i.e., the tangents of the angles). For discussion, we will only use the angle distribution.

(iii) Correlation length ξ

The correlation length measures the minimum distance from which one can consider that two points have independent heights. This distance is generally difficult to measure. It is possible to get it from the normalized autocorrelation function. Its expression for discrete mono-variate tables with M elements is

$$\rho(x_j) = \sum_{i=0}^{M-j-1} z_i z_{j+1} \Big/ \sum_{i=0}^{M-1} z_i^2, \qquad j = 0, M-1, \tag{31}$$

where z_i is the altitude at the x_i abscissa. Then we have

$$\xi = \rho^{-1}(1/e). \tag{32}$$

Therefore, it is a priori possible to estimate ξ by a dichotomy method (ρ is decreasing in the concerned interval), but there are two main problems:

- each iteration requires an important calculation time, which is nearly prohibitive for our problem;
- for very great values of M, numerical imprecisions appear in the division of the two sums in (31), because values of these sums are very important while the division is near 1.

To avoid these problems, it is possible to use known models of ρ. Two main models can be used (Ulaby *et al.*, 1986):

the gaussian model:

$$p(x) = e^{-x^2/\xi_1^2} \tag{33a}$$

a little more complex model:

$$\rho(x) = (1 + x^2/\xi_2^2)^{-3/2} \tag{33b}$$

Then we know that

$$\theta_{\text{rms}}^2 = -h_{\text{rms}}^2 \rho''(0) , \tag{34}$$

so that

$$\xi_1 = 2^{1/2} h_{\text{rms}}/\theta_{\text{rms}} \tag{35a}$$

and

$$\xi_2 = (3/2)^{1/2} \xi_1 \approx 1.22 \xi_1 . \tag{35b}$$

We have decided to calculate ξ from (31) only for the lines I_i ($i = 1, 5$), and to compare it with estimates given by (35). So we hope that found relations will allow to give ξ for the final table from its estimates from (35)

The last problem is to determine two-dimensional asteroidal characteristics from mono-variate ones:

(i) for altitudes, there is no problem: we suppose that the final table is representative of the asteroid, so all the statistical results for heights are valid and unchanged for the case of bi-variate analysis;

(ii) the problem of slopes is different: slopes that we calculate in the simulations are along the line axis. In fact we know the slopes in the perpendicular direction too. So, we could give the two-dimensional slopes from

$$\theta_b = \cos^{-1}[\cos(\theta_x) \cos(\theta_y)] . \tag{36a}$$

For small slopes, this expression can be rewritten as

$$\theta_b^2 \approx \theta_x^2 + \theta_y^2 . \tag{36b}$$

But none of these expressions can be calculated 10^9 times in reasonable time. So, we will give only mono-variate values for the mean absolute slope and the slope distribution.

However, it is necessary to estimate the rms two-dimensional slope for comparisons of our model to values obtained from real radar measurements. In fact, it is possible if we assume that:

- all angles are small. We will see that it is generally, but not always, the case;
- the slope distributions upon the x- and the y-axis are independent. It can be not true for a single crater (for example, maximum slopes on the x-axis near the top of the rim corresponds to null slopes in the perpendicular direction), but we can consider that it is true for the final distribution, because combinations of craters, plus their eradication and erosion, greatly redistributes the slopes.

Thus, for small angles we can approximate $\tan(\theta)$ by θ; and since mean slope is zero, we simply have

$$\theta_{b\,\mathrm{rms}}^2 = \int \theta_b^2 P_b(\theta_b)\,\mathrm{d}\theta_b\,, \tag{37}$$

where P is the probability density function of two-dimensional slopes. Since slopes along x- and y-axis are independent, Equation (37) yields (using relation 36b):

$$\theta_{b\,\mathrm{rms}}^2 = \int\int (\theta_x^2 + \theta_y^2) P_x(\theta_x) P_y(\theta_y)\,\mathrm{d}\theta_x\,\mathrm{d}\theta_y =$$

$$= \int \left(\int \theta_x^2 P_x(\theta_x)\,\mathrm{d}\theta_x \right) P_y(\theta_y)\,\mathrm{d}\theta_y +$$

$$\int \left(\int \theta_y^2 P_y(\theta_y)\,\mathrm{d}\theta_y \right) P_x(\theta_x)\,\mathrm{d}\theta_x\,. \tag{38}$$

Since we have

$$\int P_i(\theta_i)\,\mathrm{d}\theta_i = 1\,, \tag{39}$$

the expression (38) yields

$$\theta_{b\,\mathrm{rms}} = (\theta_{x\,\mathrm{rms}}^2 + \theta_{y\,\mathrm{rms}}^2)^{1/2} = 2^{1/2}\theta_{x\,\mathrm{rms}}\,, \tag{40}$$

which is a very simple expression that we will use in the following section;

(iii) for the length correlation, Equations (35) and (40) yield

$$\xi_{ib} = 2^{-1/2}\xi_{ix}\,. \tag{41}$$

4.2. Results

Results will be given for asteroids from 5 to 1000 km in diameter. However, results for the largest asteroids are only tentative. We will only give two-dimensional values, resulting from corrections described in Section 4.1. For each asteroid, three independent computations were made, with a variation in the initial random number as the only change. Results did not show variations greater than about 8%. For the mean values presented here, we will then admit that uncertainties do not exceed 5% (1 sigma).

Mean heights and r.m.s. heights are presented in Figures 8 and 9. For convenience, the mean height is in fact a mean depth, because all mean heights are negative. The zero-level corresponds to the hypothetical non-cratered surface. Up to about 100 km in diameter, the curves seem to be parallel. C-type asteroids have smoother surfaces than S-type asteroids, which have slightly smoother surfaces than M-type asteroids. This may be related to the depth of the regolith, which is more important for C-type asteoroids than for S-types and M-types.

For larger C-type asteroids, mean and r.m.s. heights gently decrease, which

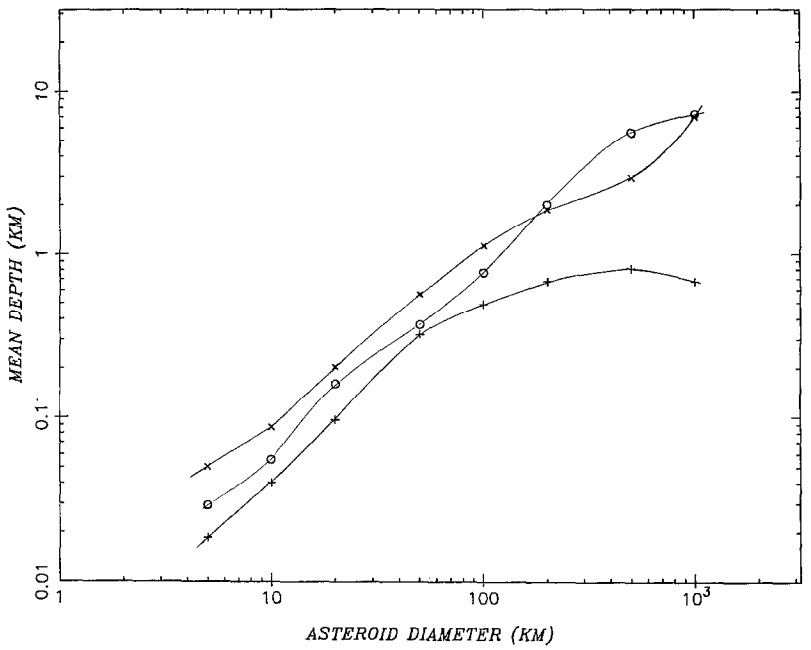

Fig. 8. Mean depths of asteroids (these values correspond to negative heights). The zero-level is for uncratered surface.

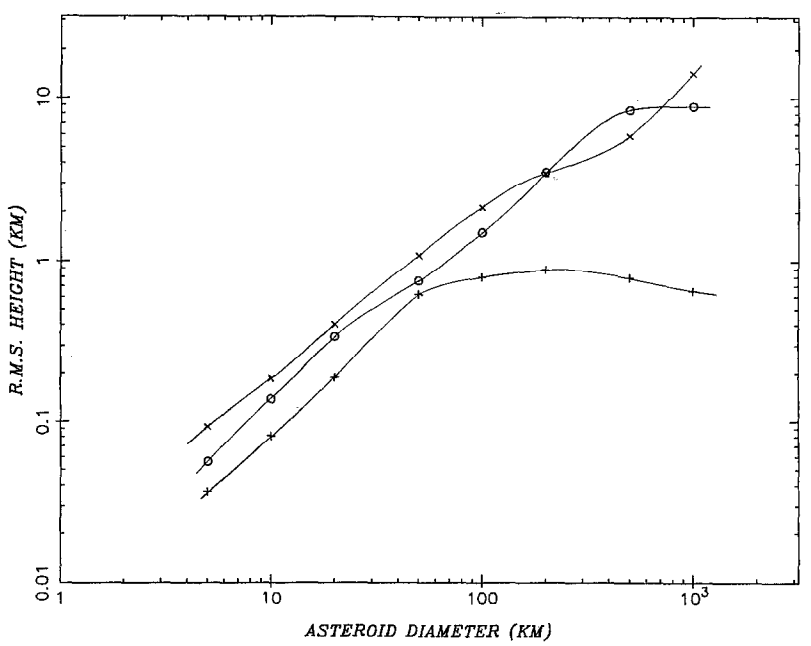

Fig. 9. R.m.s. heights of asteroids.

seems surprising. The regolith depth tends to a limiting value, so more cratered surfaces should give greater r.m.s. heights. However, as it is easily seen in Figure 3a, the crater morphology evolves toward the third type of crater, i.e. more degraded craters than for the second type. While the surface does not seem to change at metric scales, craters of several kilometers in diameter become slightly smoother as the asteroid diameter increases.

The comparison between S-type and M-type asteroids is more difficult to analyse. It results from greater depths of regolith for the big M-type asteroids than for the S-types, while the influence of the third type of crater is not clearly seen in Figures 3b and c.

Figure 10 presents results for r.m.s. slopes. Curves shows oscillations which we consider real because they are present on three independent computations, and therefore do not represent statistical variations. The values are much greater than for the Moon (computations for the Moon give a r.m.s. slope of about 8.5 deg), which is not surprising since we know (cf., Section 3.3) that asteroidal surfaces are much more cratered than lunar ones.

Up to 50 km in diameter, the general tendency is the same for r.m.s. slopes as for r.m.s. heights. The difference doesn't exceed one or two degrees, which is too small to allow a future classification of asteroids by their r.m.s. slopes. The C-type asteroids larger than 50 km in diameter have smaller r.m.s. slopes, certainly for the same reasons as those for r.m.s. heights. A behaviour of S-type asteroids

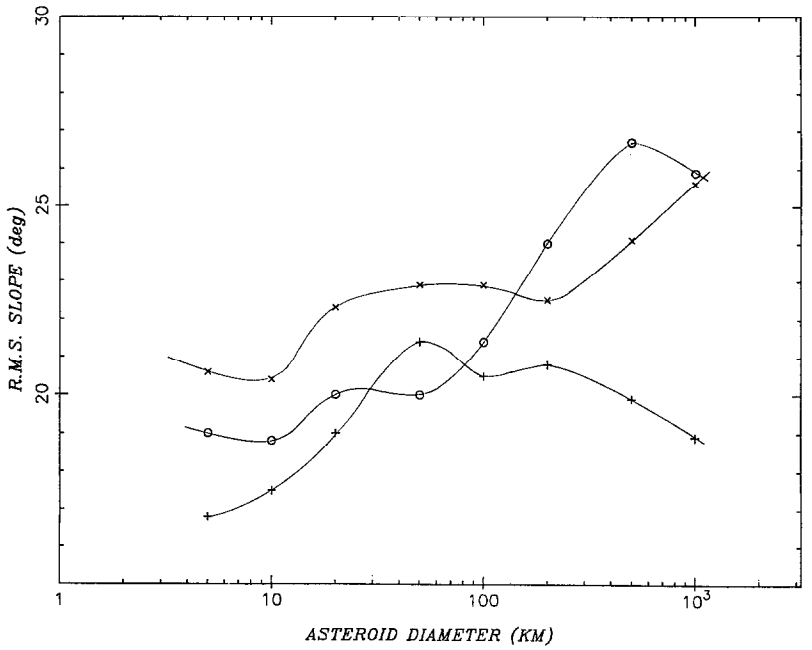

Fig. 10. R.m.s. slopes of asteroids. Note the very high obtained values.

and M-type ones is inverted from and above 100 km in diameter, and similar values are obtained for 1000 km asteroids.

The erosion parameter ϵ is certainly the most uncertain parameter of our simulations. To study its influence, we made simulations (only for S-type asteroids) with an erosion parameter two times smaller and two times greater than the 'optimal' one. Figure 11 presents r.m.s. slopes that have been obtained for the three values of ϵ. It shows that variations of about 15% are observed (the same relative variations are found for r.m.s. heights). However, mature craters are clearly too young and old craters too old when the erosion parameter is respectively two times smaller and two times bigger than the chosen value. Several simulations performed lead us to think that this value doesn't differ from the 'real' one by more than 20%, which corresponds to variations in r.m.s. slopes or heights less than 3%.

Results about the correlation lengths (as defined in Section 4.1) are presented in Figure 12. Simulations show that the direct calculation of the correlation length gives values which are always greater than the values estimated from a gaussian model. Minimum differences yield values 10% greater than gaussian values, while maximum differences correspond to values 80% greater than gaussian ones. So, for the gaussian two-dimensional values presented here, we can only say that the real values are probably no more than 40% greater. Relative classification of the

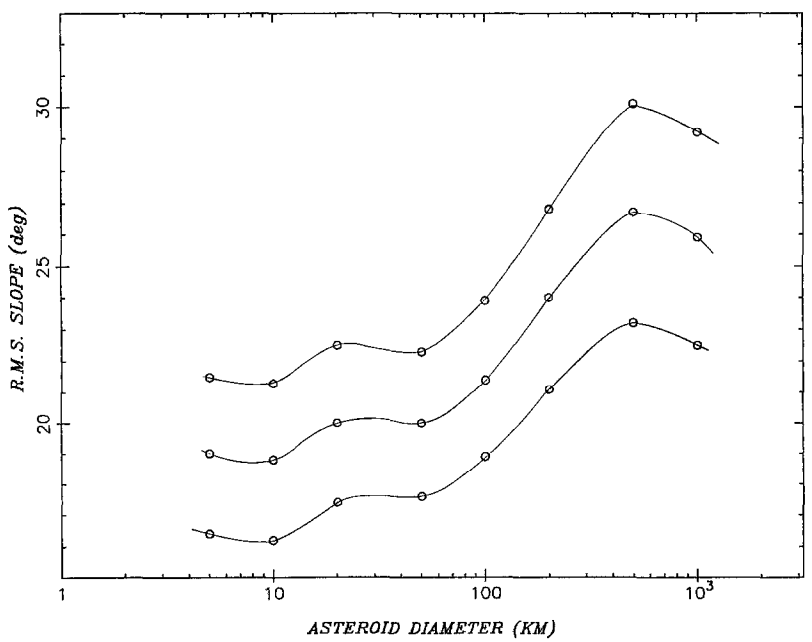

Fig. 11. R.m.s. slopes of S-type asteroids obtained with the 'optimal' (middle curve) value of the erosion parameter, and values two times smaller (top curve) and two times greater (bottom curve).

curves is certainly real, since it is correlated to the r.m.s. heights. In fact, the influence of the r.m.s. slopes is not important, because of their small variations relative to r.m.s. heights. It is interesting to note that the correlation lengths are always much greater than the wavelength of any radar, and two to three times greater than the r.m.s. heights.

Finally, we present in Figures 13 and 14, as an example, the height and slope distributions for a S-type asteroid about 500 km in diameter, and in Figures 15 and 16 the same results for simulations of the Moon.

It is important to note that we have used for these curves logarithmic scales for normalized densities, due to the very small abundances of the non zero heights or slopes. To obtain about the same number of points for the height distributions, we chose a 100 m step for the Moon and a 500 m step for the asteroid, since the height distribution is much narrower for the Moon than for the asteroid. We know that the 500 km S-type asteroid is much more cratered than the Moon and so very large depths can be obtained. But they represent very rare events, and if we search for the depth for which the probability is, for example, 1%, we find about 200 m for the Moon and 12 km for the asteroid. Positive altitudes, due in our simulations only to the top of crater rims, rapidly decrease and the 1% probability corresponds to about 200 m for the Moon and 1.7 km for the asteroid.

Abundances for the null slopes in the slope distributions are interesting to compare: this density is about 5 times greater for the Moon than for the asteroid.

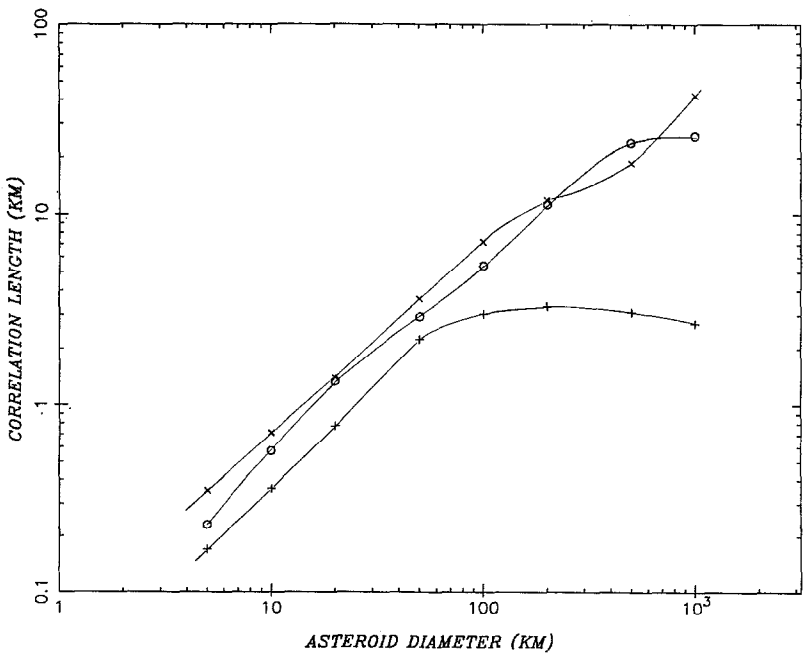

Fig. 12. Correlation lengths of asteroids. Note the likeness to the r.m.s. heights (Figure 9).

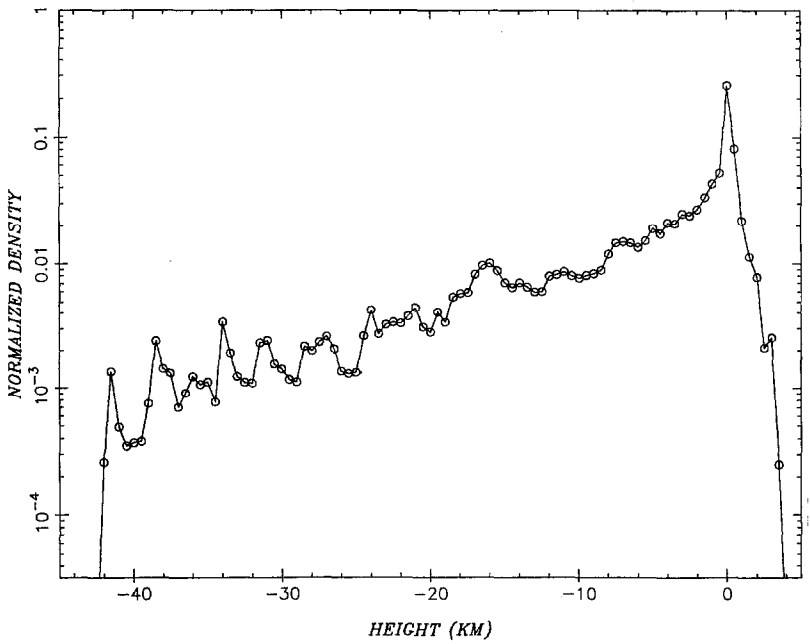

Fig. 13 Height distribution of a S-type asteroid 500 km in diameter. For Figures 13 to 16, note the log scale for the y-axis. Note the very great abundance of the near-zero heights.

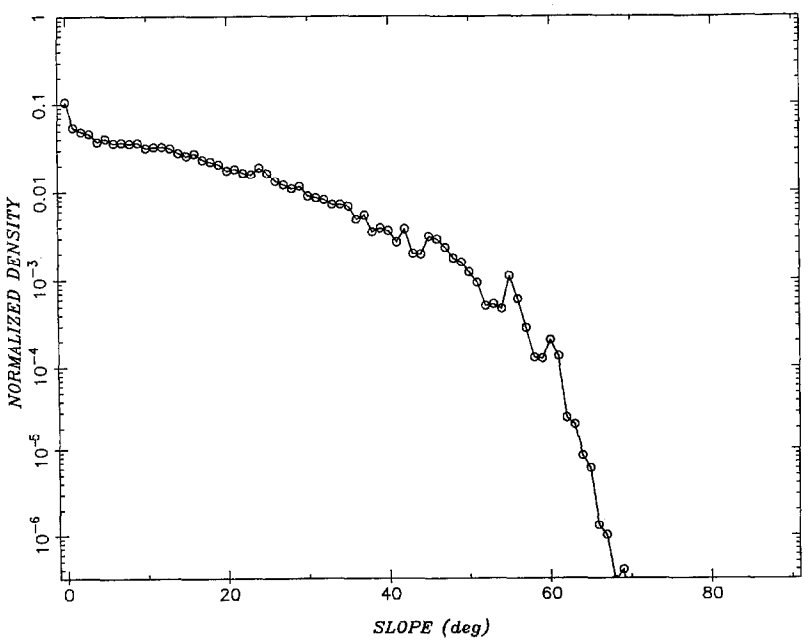

Fig. 14. Mono-dimensional slope distribution of the same asteroid than for Figure 13.

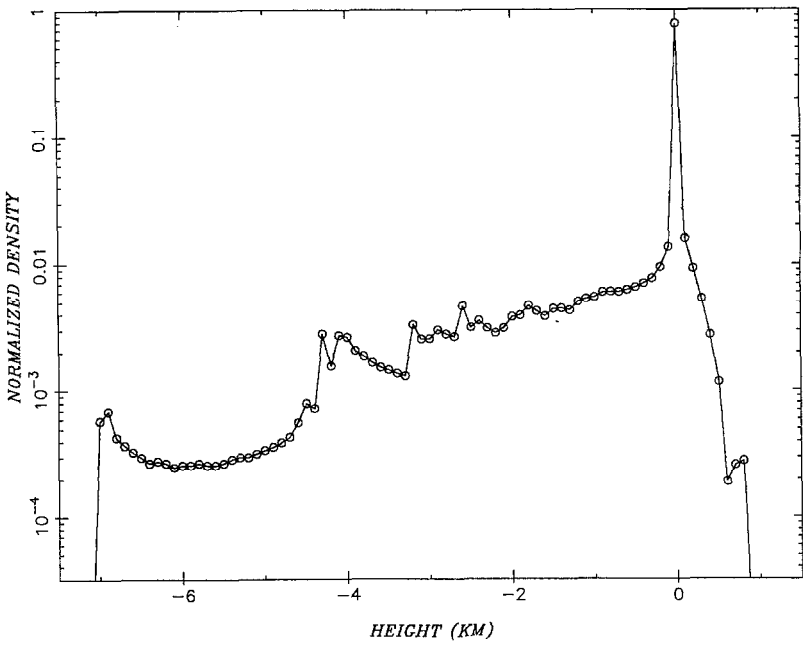

Fig. 15. Height distribution of the Moon. Compare abundances with Figure 13.

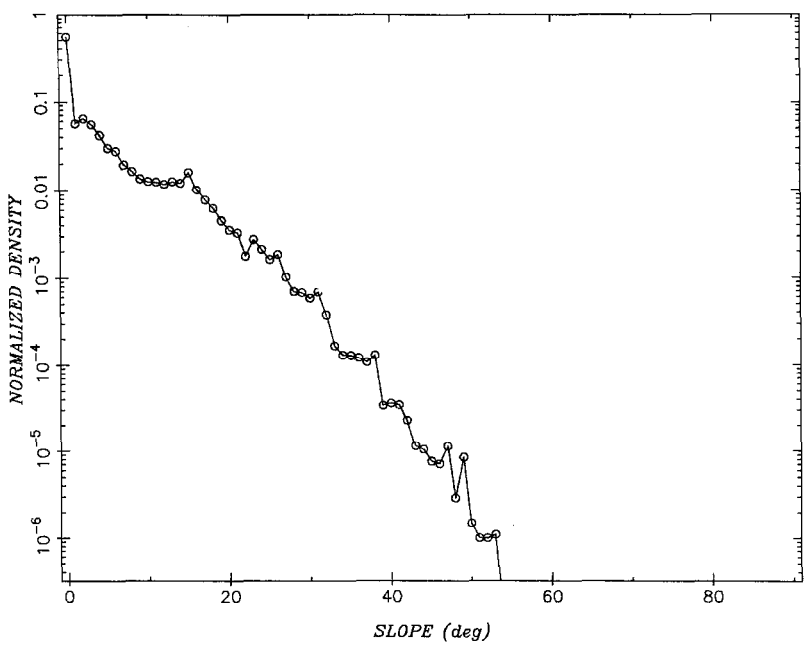

Fig. 16. Mono-dimensional slope distribution of the Moon. Note the very near 1 density for the 'flat' surfaces. Compare to Figure 14.

The 1% density yields about 16 deg for the Moon and 30 deg for the asteroid. But the most important result is certainly the shape of these distributions with the logarithmic scales of Figures 14 and 16:

- for the Moon, this shape is not far from a straight line, which corresponds to an exponential slope distribution;
- for the 500 km S-type asteroid, there is a parabolic shape, which corresponds to a Gaussian slope distribution.

This difference can be certainly explained by the fact that the asteroid surface has received much more impacts than the lunar surface. We believe that the slope distribution tends to a Gaussian law when the number of impacts becomes great enough.

5. Discussion

5.1. Influence of the particle size distribution

We have seen that the simulations presented in this paper are adapted to a centimetric radar wavelength (i.e., about 1 to 10 cm). But we only took the influence of craters and the depth of regolith into account. We must now discuss the influence of roughness of a 'typical square meter' of any simulated asteroid, which will be called microroughness in the following. This corresponds to the contribution of small or big boulders, and down to small particles of several millimeters (due to the $\lambda/10$ sampling).

It is difficult to simulate this square meter, mainly because of the three-dimensional spatial arrangement of grains. For this reason, geometrical and radar studies are actually made (Thouvenot *et al.*, in prep.) with real square meters of appropriate materials, and with various grain size distributions (mean particle size from several millimeters up to ten centimeters) and porosities. For valid statistical distributions of grains, the maximal boulder size in our samples is about 10 to 20 cm. So, we will not take bigger boulders into account, and we will consider that they are rare enough on the surface of any asteroid that their influence on heights or slopes distributions can be neglected.

In this paper, we will only give estimates of the contribution of this regolith grain size distribution. Of course, we can easily affirm that its contribution on the height distribution is null, and so the mean heights and r.m.s. heights are not modified by the regolith grain size distribution.

On the other hand, we cannot suppose that its contribution to the slope distribution is negligible. To a first approximation, we consider that the slope distribution of the regolith is independent of the slope distribution of the underlying ground, and we then admit that the 'very small scale slopes' (the regolith slopes) and the 'other scale slopes' (the simulated slopes) are simply added quadratically.

The r.m.s. slope due to the microroughness on the Moon can be estimated from Apollo mission data. Its value does not exceed 5 deg and is generally of 2 or 3 deg.

Aspects of lunar regolith have been discussed elsewhere (e.g., Langevin and Arnold, 1977), but the estimate of the grain size distribution of an asteroidal regolith is more difficult to predict (e.g., Langevin, 1982). Of course, it mainly depends on the strength of the material, because it is easier to obtain fine-grained particles with a weak material than with a strong one. This is in good agreement with Earth-based radar estimates of the centimetric smoothness of several asteroids (e.g., Ostro *et al.*, 1985). According to these results, at a centimer scale, C-type and S-type asteroids seem not much rougher, and are sometimes much smoother, than the Moon. Extrapolations to M-type asteroids might be uncertain, but we will assume that the upper limit for the r.m.s. slope of the microroughness of any asteroid is, say, 5 deg.

If we calculate the miminum slope necessary to increase quadratically a 15 deg r.m.s. slope by only 1 deg, we find a little less than 6 deg (and more than 9 deg for a r.m.s. slope of 30 deg). So, we will consider in the following that the contribution of the regolith grain size distribution to the r.m.s. slope of any asteroid is smaller than 1 deg.

5.2. Comparisons with observational data

In this section, we present three different comparisons of the results of our simulations with observational data. The main problem is the lack of data for asteroidal surfaces.

(a) *R.m.s. Slope on the Moon*

Values of r.m.s. slope for the Moon at various radar wavelengths have been compiled by Pettengill (1978). We will not take the value (33 deg) at 0.86 cm into account because it is much higher than all other values given elsewhere in the literature and then seems doubtful. The most interesting value is 9.1 deg for a 3.5 cm wavelength (Evans, 1969), which is correlated with values of 7.1 and 5.9 deg at respectively 23 cm and 70 cm wavelength (Hagfors, 1970).

R.m.s. slope given by the simulations for the Moon is 8.5 deg. If we suppose that the contribution of the regolith grain size distribution is between 2 and 5 deg, final values for the r.m.s. slope is between 8.7 and 9.4 deg. It fits very well with observational results at centimetric wavelengths.

(b) *Maximum Heights on an Asteroid*

Estimates of asteroidal heights are very rare. Effective resolution of speckle interferometry is not yet good enough to obtain results about altitudes on asteroids (e.g., Drummond *et al.*, 1988). An interesting technique to get information about altitudes on their limbs might be the occultations by stars. Unfortunately, residuals of observations after the estimate of the profile of the asteroid are difficult to interpret in terms of altitudes above or below the mean surface (e.g., Millis *et al.*, 1985). Increasing the timing accuracy will certainly reduce the uncertainties about these residuals.

The case of Phobos provides an interesting comparison. Of course, Phobos has particular physical characteristics, so we have to take values given in the literature

for our simulations. In particular, we have used crater densities given by Thomas and Veverka (1980). In his model of Phobos, Turner (1978) concludes that the greatest elevation difference on Phobos is about 3.2 km, which seems very important because it represents about 30% of its mean radius.

Our simulations of Phobos lead to a maximum variation in elevation of about 1.7 km. It corresponds in a maximal depth of about 1.45 km and a maximal height of 0.25 km. Thus if the lowest elevation is in good agreement with Turner's value (1.6 km), our model does not simulate the highest altitudes (1.6 km). For Phobos, it corresponds to the extremely high raised rim of Stickney (more than 1 km), which seems enormous and may be due to particular geological processes during this impact, i.e. a nature consequence of impact mechanisms on an ellipsoidal body of this size.

However, high positive altitudes are very rare on the surface and certainly do not deeply affect the slope and height distributions. On the other hand, this example points out an important potential problem for radar altimetric studies of small asteroids: the possibility of having such an irregular shape that topography becomes uncertain.

(c) *R.m.s. Slopes on Asteroids*

About fifty asteroids have been observed by Earth-based radar, but we know only one estimate of the r.m.s. slope of an asteroid, Pallas, given by Ostro *et al.* (1985), which is 27 ± 3 deg at a 13 cm wavelength. But for nearly all radar observed asteroids, and each of the twenty asteroids studied by Ostro *et al.*, their surfaces are, according to these authors, "much rougher than the Moon at some scales between several meters and many kilometers" and "must have very large r.m.s. slopes".

Unfortunately, Pallas classification is not certain and may be between C and S type. For an asteroid, 530 km in diameter, our simulations give an r.m.s. slope of 19.7 and 26.6 deg for C-type and S-type respectively. These values may be incremented by about 1 degree according to Section 5.1, which leads to 21 deg for C-type and 28 deg for S-type, with an uncertainty of about 1.5 deg. On the other hand, observational values have to be slightly increased (certainly by less than 2 deg) in order to correspond to centimetric wavelengths.

So, the only conclusion that we can give is that our simulations are in good agreement with Pallas observations only if its material has the same mechanical properties as S-type material. For our simulations, the most important point is the crust composition, and it does not exclude an upper layer or a regolith with a different composition. Since Pallas seems nearly spherical, it may have been differentiated. The density of Pallas, 2.8 ± 0.5 g cm^{-3} (Wasserman *et al.*, 1979), is compatible with the existence of a stony material on or near the surface.

6. Conclusions

Mono-dimensional simulations of asteroidal surfaces may be realized with good precision by computer simulations. A limited number of physical considerations

provides an estimate of the evolution of the surface of minor planets. However, the results are restricted to non-differentiated asteroids, because the geological consequences of melting the surface are difficult to predict precisely.

The model presented here contains several free parameters, which could lead to uncertain results. However, although uncertainties about asteroids preclude a good estimate of these parameters, the case of the Moon may be very useful. Of course, it must be done with caution because the Moon is physically different from an asteroid, but its surface is much more precisely known than that of any asteroid.

Simulations confirm these great differences between the Moon and asteroids. Surfaces of asteroids are extremely cratered, saturated for nearly all crater diameters. They are generally covered with a layer of regolith, but its thickness greatly depends on the type and the diameter of the asteroid. In spite of erosion, r.m.s. slopes and heights given by the simulations depend on cratering. They correspond to much rougher surfaces than on the Moon, at metric or larger scales, as suggested from radar observations.

Comparisons with observational results are difficult because of the lack of data, but the simulations seem realistic. The main problem for their applications to bi-dimensional simulations is the optimization of the algorithm to avoid prohibitive computer times. The results of our first attempts allow us to be optimistic on this point.

Acknowledgements

We thank Dr P. Masson for correcting a first version of this paper, and Dr Y. Langevin for his very useful advices.

This work is supported through a M.R.T.-Alcatel Espace grant.

References

Croft, S. K.: 1985, Proc. 15th Lunar Planet. Sci. Conf., *J. Geophys. Res.* **90**, C828–C842.
Davis, D. R. *et al.*: 1985, *Icarus* **62**, 30–53.
Drummond, J. *et al.*: 1988, *Icarus*, **73**,1–14.
Evans, J. V.: 1969, *Ann. Rev. Astron. Astroph.* **7**, 201–248.
Gault, D. E. and Wedekind, J. A.: 1977, *Impact and Explosion Cratering*, Pergamon Press (NY), pp. 1231–1244.
Goldstein, R. M.: 1968, *Science* **162**, 903–904.
Goldstein, R. M.: 1969, *Icarus* **10**, 430–431.
Hagfors, T.: 1970, *Radio Sci.* **5**, 189–227.
Hartmann, W. K.: 1977, *Icarus* **31**, 260–276.
Hartmann, W. K.: 1984, *Icarus* **60**, 65–74.
Helfenstein, P.: 1988, *Icarus* **73**, 462–481.
Housen, K. R. *et al.*: 1979a, *Icarus* **39**, 317–351.
Housen, K. R. *et al.*: 1979b, in T. Gehrels (ed.), *Asteroids*, Univ. Ariz. Press, pp. 601–627.
Housen, K. R.: 1981, *Advances in Planetary Geology*, NASA-TM-84412, pp. 3–217.
Housen, K. R. and Wilkening, L. L.: 1982, *Ann. Rev. Earth Planet. Sci.* **10**, 355–376.
Langevin, Y. and Arnold, J. R.: 1977, *Ann. Rev. Earth Planet. Sci.* **5**, 449–489.
Langevin, Y. and Maurette, M.: 1980, *Lunar Planet. Sci.* **XI**, 602–604.

Langevin, Y. and Maurette, M.: 1981, *Lunar Planet. Sci.* **XII**, 595–597.
Langevin, Y.: 1982, *Meteoritic Breccias and Lunar Analogs*, Lunar Planet. Instit., pp. 87–93.
Langevin, Y.: 1986, 1st Internat. Coll. Mission Phobos, Moscow.
Malin, M. C. and Dzurisin, D.: 1977, *J. Geophys. Res.* **82**(2), 376–388.
Millis, R. L. *et al.*: 1985, *Icarus* **61**, 124–131.
Moore, H. J. *et al.*: 1980, *Moon and Planets* **23**, 231–252.
Ostro, S. J. *et al.*: 1985, *Science* **229**, 442–446.
Perret, A. *et al.*: 1988, Vesta: Phase A Report, C.N.E.S.
Pettengill, G. H. *et al.*: 1969, *Icarus* **10**, 432–435.
Pettengill, G. H.: 1978, *Ann. Rev. Astron. Astroph.* **16**, 265–292.
Pike, R. J.: 1977, *Impact and Explosion Cratering*, Pergamon Press (NY), pp. 489–509.
Raizonville, P. *et al.*: Proceedings if IGARSS '88 Symposium, ESA-SP-284, pp. 977–979.
Ravine, M. A. and Grieve, R. A. F.: 1986, Proc. 17th Lunar Planet. Sci. Conf., *J. Geophys. Res.* **91**, B13, pp. E75–E83.
Sotor, L.: 1971, Cent. Radiophys. Space Res. Rep. 462, Cornell Univ., Ithaca, NY.
Thomas, P. and Veverka, J.: 1980, *Icarus* **41**, 365–380.
Turner, R. J.: 1978, *Icarus* **33**, 116–140.
Ulaby, R. T. *et al.*: 1986, *Microwave Remote Sensing*, Artech House Inc.
Veverka, J.: 1978, *Vistas in Astronomy* **22**, 163–192.
Wasserman, L. H. *et al.*: 1979, *Astron. J.* **84**, 259–268.
Wood, C. A. and Andersson, L.: 1978, Proc. Lunar Planet. Sci. Conf. 9th, pp. 3669–3689.